Computer Assisted Mechanics and Engineering Sciences, 7: 435–448, 2000.

General FEM model of prestressing tendons

Daniel Antoniak and Piotr Konderla
Institute of Civil Engineering, Wrocław University of Technology,
Wybrzeże Wyspiańskiego 27, 50-370 Wrocław, Poland

(Received November 3, 1999)

The paper presents a general numerical model for the analysis of prestressed concrete with the application to beam, thin shell and volume type of prestressed structures. Discrete, embedded approach is used to model curved, bonded or unbonded tendons. Also a partial bond may be introduced by the friction between the tendon and the surrounding body. In the finite element model, two types of elements are obtained. One is a typical finite element for the kind of structure modeled, and the other is an embedded, three noded, subparametric tendon element. Equations of the finite element method have been obtained from the incremental form of the principle of virtual work providing geometrical linearity and possibility of nonlinear physical relations. Numerical examples illustrate application to modeling of beam, thin shell and volume type of prestressed structures as well as the impact of the friction on the axial force distribution in prestressing tendon.

1. Introduction

A general numerical model for the analysis of prestressed concrete structures is presented. The paper is an extension of previous contributions of the authors [2, 3, 4] in which physical and numerical models of slabs and shells were described. Application to modeling of beam, thin shell and volume type of prestressed structures is shown. From the physical modeling point of view these are respectively one-, two- and three-dimensional bodies. Tendons are assumed to be embedded in a body with the possibility of independent slip i.e. displacement in the direction tangent to the tendon. The friction between the tendon and the surrounding body may constrain the slip and introduce prestressing loss, but unlike in other formulations known in literature [8, 13, 17, 18], neither analytical solution for friction is used nor any additional link is needed to solve the problem.

When finite element method is applied, two types of elements are obtained. One is a typical finite element for the kind of structure modeled, referred to as a parent element, and the other is an embedded, three nodded, subparametric tendon element. Its geometry is approximated with square polynomials on the basis of three nodes, coordinates of which are determined with respect to the parent element. The total displacement of the tendon is assumed to be a sum of the parent element movement and the independent slip, which is approximated between nodes with linear functions independently on the two segments of the element.

Formulating the model, the attention was mainly focused on the description of the tendon element and its compatibility with the parent element. It has been achieved by modification of the original [5, 15] embedded approach. Equations of the finite element method have been obtained from the incremental form of the principle of virtual work providing geometrical linearity and possibility of nonlinear physical relations. Nonlinearity arises also from friction posing a contact problem between the parent and the embedded elements.

The impact of friction on axial force distribution in prestressing tendon will be shown in numerical examples and compared to analytical solution. Other examples will illustrate application of the model to beam, thin shell and volume type of prestressed structures.

2. Discrete model of a prestressed structure

2.1. Parent element

The geometry of the parent element described by the position radius-vector $\mathbf{r}$ is approximated with the use of a geometry shape function matrix $\mathbf{N}$ and vectors of the parent element nodal coordinates $\mathbf{x}_\alpha$ in the following way

$$\mathbf{r}(\boldsymbol{\xi}) = \mathbf{N}_\alpha(\boldsymbol{\xi})\mathbf{x}_\alpha\,, \tag{1}$$

where $\boldsymbol{\xi}$ is a vector of parent element local parameters. Depending on the type of element, $\mathbf{r}$ may refer to any point within the parent element or to some reference level like neutral axis in beams or middle surface in shells. To avoid this ambiguity, let $\hat{\mathbf{r}}$ always refer to any point of the parent element. It will either be equal to $\mathbf{r}$ or will be some modification of $\mathbf{r}$. Similarly, displacement field

$$\mathbf{u}(\boldsymbol{\xi}) = \mathbf{L}_\alpha(\boldsymbol{\xi})\mathbf{q}_\alpha \tag{2}$$

interpolated by displacement shape functions $\mathbf{L}_\alpha$ and nodal displacements $\mathbf{q}_\alpha$ may refer to the reference level whereas

$$\hat{\mathbf{u}}(\boldsymbol{\xi}) = \hat{\mathbf{L}}_\alpha(\boldsymbol{\xi})\mathbf{q}_\alpha \tag{3}$$

always denotes displacement of any point within parent element and is interpolated with functions $\hat{\mathbf{L}}_\alpha$.

An operator of geometrical relations $\mathcal{B}$ applied to the displacement field yields matrix of strain-displacement relations $\mathbf{B}$. Thus, a vector of strains can be expressed by

$$\boldsymbol{\varepsilon}(\boldsymbol{\xi}) = \mathcal{B}[\mathbf{u}(\boldsymbol{\xi})] = \mathbf{B}_\alpha(\boldsymbol{\xi})\mathbf{q}_\alpha\,, \tag{4}$$

with $\mathbf{B}_\alpha(\boldsymbol{\xi}) = \mathcal{B}[\mathbf{L}_\alpha(\boldsymbol{\xi})]$. A material model is assumed that can be described with the differential relation between stresses and strains

$$\mathrm{d}\boldsymbol{\sigma} = \mathbf{D}\,\mathrm{d}\boldsymbol{\varepsilon}\,, \tag{5}$$

where $\mathbf{D} = \mathbf{D}(\boldsymbol{\varepsilon})$ is a matrix of tangential stress-strain relations. To obtain incremental equations of equilibrium the following approximation is used

$$\Delta\boldsymbol{\sigma} = \mathbf{D}\,\Delta\boldsymbol{\varepsilon}\,. \tag{6}$$

This approach is justified to derive the stiffness matrix, which does not need to be exact. On the other hand it enforces small increments, especially if larger nonlinearities are encountered. To avoid this inconvenience the stress increments are calculated explicitly

$$\Delta\boldsymbol{\sigma} = \int_{\boldsymbol{\varepsilon}}^{\boldsymbol{\varepsilon}+\Delta\boldsymbol{\varepsilon}} \mathbf{D}(\boldsymbol{\varepsilon})\mathrm{d}\boldsymbol{\varepsilon}\,. \tag{7}$$

2.2. Embedded tendon element

Two approaches are used in the modeling of embedded tendon elements [4, 8, 9, 17]. Tendon location may be first approximated either in the global coordinates and then mapped to the local frame of the parent element or first in the local one and then transformed to the global system using parent element shape functions. The latter approach is proposed here.

Assuming that we know local parent element coordinates of the embedded tendon nodes $\hat{\boldsymbol{\xi}}_\beta$, the interpolation of the tendon course in parent element local coordinates may be written as

$$\tilde{\boldsymbol{\xi}}(\vartheta) = \tilde{N}_\beta(\vartheta)\hat{\boldsymbol{\xi}}_\beta\,, \tag{8}$$

with $\vartheta \in \langle -1, 1\rangle$ being tendon element local parameter and tendon geometry shape functions

$$\tilde{\mathbf{N}}(\vartheta) = [\tilde{N}_1(\vartheta), \tilde{N}_2(\vartheta), \tilde{N}_3(\vartheta)] = [-\vartheta(1-\vartheta)/2\,,\ 1-\vartheta^2\,,\ \vartheta(1+\vartheta)/2]\,. \tag{9}$$

Now the tendon position radius-vector $\tilde{\mathbf{r}}(\vartheta)$ in global coordinates can be derived from the parent element

$$\tilde{\mathbf{r}}(\vartheta) = \hat{\mathbf{r}}(\tilde{\boldsymbol{\xi}}(\vartheta))\,, \tag{10}$$

and then the tendon tangent and normal base vectors may be calculated. Respectively we obtain

$$\tilde{\mathbf{g}} = \frac{\mathrm{d}\tilde{\mathbf{r}}/\mathrm{d}s}{|\mathrm{d}\tilde{\mathbf{r}}/\mathrm{d}s|}\,, \tag{11}$$

$$\tilde{\mathbf{n}} = \frac{\mathrm{d}\tilde{\mathbf{g}}/\mathrm{d}s}{|\mathrm{d}\tilde{\mathbf{g}}/\mathrm{d}s|}\,, \tag{12}$$

where $\mathrm{d}s$ is the tendon arc element. The curvature of the tendon can be determined from the formula

$$|\tilde{\kappa}(\vartheta)| = \sqrt{\frac{\mathrm{d}\tilde{\mathbf{n}}}{\mathrm{d}s} \cdot \frac{\mathrm{d}\tilde{\mathbf{n}}}{\mathrm{d}s}}\,. \tag{13}$$

The total tendon displacement is the sum of the parent element displacement $\hat{\mathbf{u}}(\boldsymbol{\xi}(\vartheta)) = \hat{\mathbf{L}}_\alpha(\boldsymbol{\xi}(\vartheta))\mathbf{q}_\alpha$ at the tendon location and the tendon slip v relative to the parent element in the direction of $\tilde{\mathbf{g}}(\vartheta)$

$$\tilde{\mathbf{u}}(\vartheta) = \hat{\mathbf{u}}(\boldsymbol{\xi}(\vartheta)) + \tilde{\mathbf{g}}(\vartheta)\tilde{L}_\beta(\vartheta)v_\beta\,, \tag{14}$$

where the slip is interpolated betweeen nodes with $\tilde{\mathbf{L}}$ equal to

$$\tilde{\mathbf{L}}(\vartheta) = [\tilde{L}_1(\vartheta), \tilde{L}_2(\vartheta), \tilde{L}_3(\vartheta)] = \begin{cases} [-\vartheta, & 1+\vartheta, & 0\,]\,, & \vartheta < 0, \\ [\ 0, & 1-\vartheta, & \vartheta\,]\,, & \vartheta \geq 0. \end{cases} \tag{15}$$

The axial strain in the tendon can be calculated as

$$\varepsilon(\vartheta) = \tilde{\mathbf{g}}^{\mathrm{T}}\frac{\mathrm{d}\tilde{\mathbf{u}}}{\mathrm{d}s} = \mathbf{C}_\alpha\mathbf{q}_\alpha + H_\beta v_\beta\,, \tag{16}$$

with

$$\mathbf{C}_\alpha = \tilde{\mathbf{g}}^{\mathrm{T}}\frac{\mathrm{d}}{\mathrm{d}\vartheta}\left[\hat{\mathbf{L}}_\alpha\left(\tilde{\boldsymbol{\xi}}(\vartheta)\right)\right]\left(\frac{\mathrm{d}s}{\mathrm{d}\vartheta}\right)^{-1}\,, \tag{17}$$

$$H_\beta = \frac{\mathrm{d}\tilde{L}_\beta(\vartheta)}{\mathrm{d}\vartheta}\left(\frac{\mathrm{d}s}{\mathrm{d}\vartheta}\right)^{-1}\,. \tag{18}$$

Please note that approximation proposed in Eqs. (8) and (10) facilitates differentiation with respect to $\mathrm{d}s$. Any quantity $(\cdot)$ can be differentiated according to the following rules

$$\frac{\mathrm{d}(\cdot)}{\mathrm{d}s} = \frac{\mathrm{d}(\cdot)}{\mathrm{d}\vartheta}\left(\frac{\mathrm{d}s}{\mathrm{d}\vartheta}\right)^{-1}\,, \tag{19}$$

$$\frac{\mathrm{d}s}{\mathrm{d}\vartheta} = \sqrt{\frac{\mathrm{d}\tilde{r}_i}{\mathrm{d}\vartheta}\frac{\mathrm{d}\tilde{r}_i}{\mathrm{d}\vartheta}} = \sqrt{\frac{\mathrm{d}}{\mathrm{d}\vartheta}\left[\hat{r}_i\left(\tilde{\boldsymbol{\xi}}(\vartheta)\right)\right]\frac{\mathrm{d}}{\mathrm{d}\vartheta}\left[\hat{r}_i\left(\tilde{\boldsymbol{\xi}}(\vartheta)\right)\right]}\,, \tag{20}$$

$$\frac{\mathrm{d}\tilde{\boldsymbol{\xi}}(\vartheta)}{\mathrm{d}\vartheta} = \frac{\mathrm{d}\tilde{L}_i(\vartheta)}{\mathrm{d}\vartheta}\tilde{\boldsymbol{\xi}}_i\,. \tag{21}$$

With the same provision as to Eq. (6), the incremental constitutive relation between the increments of tendon axial force N and strain ε is written as

$$\Delta N(\vartheta) = D\Delta\varepsilon(\vartheta) = D\left(\mathbf{C}_\alpha\Delta\mathbf{q}_\alpha + H_\beta\Delta v_\beta\right)\,, \tag{22}$$

with tendon axial stiffness $D = E(\varepsilon)A$ where $E(\varepsilon) = \mathrm{d}\sigma/\mathrm{d}\varepsilon$ is the tangential modulus and A is the cross section area of the tendon.

In many formulations of prestressed structure models, the loss of prestressing due to friction is determined beforehand from the well-known formula

$$N(\vartheta + \Delta\vartheta) = N(\vartheta)e^{-(\mu\Delta\phi + K\Delta s)}, \tag{23}$$

where μ and K are the curvature and wobble friction coefficients, $\Delta\phi$ is the angle change and Δs is the distance corresponding to $\Delta\vartheta$. Thus, the distribution of the prestressing force is calculated and then it is inserted as the initial axial force or load-equivalent concept is used introduce prestressing.

Here, the Coulomb type of friction between the tendon and the surrounding structure is incorporated explicitly into the model. The limit friction force T at which the slip of the tendon becomes possible equals

$$T(\vartheta) = -\mathrm{sign}(\Delta v)(T_0 + \mu\,|\kappa(\vartheta)|\,|N(\vartheta)|)\,, \tag{24}$$

with $\kappa = \tilde{\kappa} + \hat{\kappa}$, where $\hat{\kappa}$ is associated with the wobble of the tendon duct. $T_0 \geq 0$ introduces an independent of N minimum value of the friction force that has to be overcome to obtain the tendon slip. For $T_0 = 0$ Eqs. (23) and (24) conform one to another since $T = \mathrm{d}N/\mathrm{d}s$ and $\mu\hat{\kappa} = K$. Factor $-\mathrm{sign}(\Delta v)$ means that the friction force is always opposed to the direction of slip increment.

2.3. Equilibrium equations

To derive the equilibrium equations, the incremental form of the virtual work principle is used in the form of

$$\int_V \delta\Delta\mathbf{u}^{\mathrm{T}}\,(\mathbf{Q} + \Delta\mathbf{Q})\,\mathrm{d}V + \int_L \delta\Delta v\,(P + \Delta P)\,\mathrm{d}L + \int_L \delta\Delta v\,(T + \Delta T)\,\mathrm{d}L$$
$$= \int_V \delta\Delta\boldsymbol{\varepsilon}^{\mathrm{T}}\,(\boldsymbol{\sigma} + \Delta\boldsymbol{\sigma})\,\mathrm{d}V + \int_L \delta\Delta\varepsilon\,(N + \Delta N)\,\mathrm{d}L\,, \tag{25}$$

where $\mathbf{Q}$ is a vector of parent element loads and P denotes loading applied to the tendon. Variations of the quantities found in Eq. (25) can be calculated as follows

$$\delta\Delta\mathbf{u} = \mathbf{L}_\alpha\delta\Delta\mathbf{q}_\alpha\,, \tag{26}$$
$$\delta\Delta\boldsymbol{\varepsilon} = \mathbf{B}_\alpha\delta\Delta\mathbf{q}_\alpha\,, \tag{27}$$
$$\delta\Delta v = \tilde{L}_\alpha\delta\Delta v_\alpha\,, \tag{28}$$
$$\delta\Delta\varepsilon = \mathbf{C}_\alpha\delta\Delta\mathbf{q}_\alpha + H_\beta\delta\Delta v_\beta\,. \tag{29}$$

Considering (24) and introducing two factors, namely

$$S_v = \begin{cases} 1, & \Delta v \geq 0 \\ -1, & \Delta v < 0 \end{cases} \quad \text{and} \quad S_{\mathrm{N}} = \begin{cases} 1, & N + \Delta N \geq 0 \\ -1, & N + \Delta N < 0 \end{cases}, \tag{30}$$

the expression $\delta\Delta v\,(T + \Delta T)$ becomes

$$\delta\Delta v(T + \Delta T) = -\delta\Delta v\,S_{\mathrm{v}}\,(T_0 + \mu\,|\kappa|\,|N + \Delta N|) = -\delta\Delta v\,S_{\mathrm{v}}T_0 - \delta\Delta v\,\mu\,|\kappa|\,S_{\mathrm{v}}S_{\mathrm{N}}(N + \Delta N)\,. \tag{31}$$

Now, the integrals in Eq. (25) can be rewritten

$$\int_V \delta\Delta\mathbf{u}^{\mathrm{T}}\,(\mathbf{Q} + \Delta\mathbf{Q})\,\mathrm{d}V = \delta\Delta\mathbf{q}_\alpha^{\mathrm{T}}\int_V \mathbf{L}_\alpha^{\mathrm{T}}\,(\mathbf{Q} + \Delta\mathbf{Q})\,\mathrm{d}V\,, \tag{32}$$

$$\int_L \delta\Delta v\,(P+\Delta P)\,\mathrm{d}L = \delta\Delta v_\beta \int_L \tilde{L}_\beta\,(P+\Delta P)\,\mathrm{d}L\,, \tag{33}$$

$$\begin{aligned}\int_L \delta\Delta v(T+\Delta T)\,\mathrm{d}L &= -\delta\Delta v_\beta \left(\int_L \tilde{L}_\beta N S_v S_\mathrm{N}\,\mathrm{d}L + \int_L \tilde{L}_\beta \mu|\kappa| S_v S_\mathrm{N} D\,\mathbf{C}_k\Delta\mathbf{q}_k\,\mathrm{d}L\right.\\ &\quad \left. + \int_L \tilde{L}_\beta \mu|\kappa| S_v S_\mathrm{N} D\,H_n\Delta v_n\,\mathrm{d}L + \int_L \tilde{L}_\beta S_v T_0\,\mathrm{d}L\right),\end{aligned} \tag{34}$$

$$\int_V \delta\Delta\boldsymbol{\varepsilon}^\mathrm{T}\,(\boldsymbol{\sigma}+\Delta\boldsymbol{\sigma})\,\mathrm{d}V = \delta\Delta\mathbf{q}_\alpha^\mathrm{T}\left(\int_V \mathbf{B}_\alpha^\mathrm{T}\boldsymbol{\sigma}\,\mathrm{d}V + \int_V \mathbf{B}_\alpha^\mathrm{T}\mathbf{D}\,\mathbf{B}_k\Delta\mathbf{q}_k\,\mathrm{d}V\right), \tag{35}$$

$$\begin{aligned}\int_L \delta\Delta\varepsilon\,(N+\Delta N)\,\mathrm{d}L &= \delta\Delta\mathbf{q}_\alpha^\mathrm{T}\left(\int_L \mathbf{C}_\alpha^\mathrm{T} N\,\mathrm{d}L + \int_L \mathbf{C}_\alpha^\mathrm{T} D\,\mathbf{C}_k\Delta\mathbf{q}_k\,\mathrm{d}L + \int_L \mathbf{C}_\alpha^\mathrm{T} D\,H_n\Delta v_n\,\mathrm{d}L\right)\\ &\quad + \delta\Delta v_\beta\left(\int_L H_\beta N\,\mathrm{d}L + \int_L H_\beta D\,\mathrm{C}_k\Delta\mathbf{q}_k\,\mathrm{d}L + \int_L H_\beta D\,H_n\Delta v_n\,\mathrm{d}L\right).\end{aligned} \tag{36}$$

Kinematically admissible variations of independent displacement fields $\mathbf{u}$ and v can be applied separately to the virtual work principle assuming that one of them is zero. Thus, considering Eqs. (32)–(34) and canceling common factors, we have for $\delta\Delta\mathbf{u} = \mathbf{L}_\alpha\delta\Delta\mathbf{q}_\alpha$ and $\delta\Delta v = 0$

$$\begin{aligned}&\int_V \mathbf{L}_\alpha^\mathrm{T}\,(\mathbf{Q}+\Delta\mathbf{Q})\,\mathrm{d}V - \int_V \mathbf{B}_\alpha^\mathrm{T}\boldsymbol{\sigma}\,\mathrm{d}V - \int_L \mathbf{C}_\alpha^\mathrm{T} N\,\mathrm{d}L\\ &\quad = \int_V \mathbf{B}_\alpha^\mathrm{T}\mathbf{D}\,\mathbf{B}_k\Delta\mathbf{q}_k\,\mathrm{d}V + \int_L \mathbf{C}_\alpha^\mathrm{T} D\,\mathbf{C}_k\Delta\mathbf{q}_k\,\mathrm{d}L + \int_L \mathbf{C}_\alpha^\mathrm{T} D\,H_n\Delta v_n\,\mathrm{d}L\,,\end{aligned} \tag{37}$$

and for $\delta\Delta\mathbf{u} = \mathbf{0}$ and $\delta\Delta v = \tilde{L}_\beta\delta\Delta v_\beta$

$$\begin{aligned}&\int_L \tilde{L}_\beta\,(P+\Delta P)\,\mathrm{d}L - \int_L H_\beta N\,\mathrm{d}L - \int_L \tilde{L}_\beta N S_v S_\mathrm{N}\,\mathrm{d}L\\ &\quad = \int_L H_\beta D\,\mathrm{C}_k\Delta\mathbf{q}_k\,\mathrm{d}L + \int_L \tilde{L}_\beta\mu|\kappa| S_v S_\mathrm{N} D\,\mathbf{C}_k\Delta\mathbf{q}_k\,\mathrm{d}L +\\ &\quad + \int_L H_\beta D\,H_n\Delta v_n\,\mathrm{d}L + \int_L \tilde{L}_\beta\mu|\kappa| S_v S_\mathrm{N} D\,H_n\Delta v_n\,\mathrm{d}L + \int_L \tilde{L}_\beta\mu S_v T_0\,\mathrm{d}L\,.\end{aligned} \tag{38}$$

Finally, Eqs. (37) and (38) may be combined together to form a compact matrix equation

$$\left[\begin{array}{c|c} \displaystyle\int_V \mathbf{B}_\alpha^\mathrm{T}\mathbf{D}\mathbf{B}_k\,\mathrm{d}V + \int_L \mathbf{C}_\alpha^\mathrm{T} D\,\mathbf{C}_k\,\mathrm{d}L & \displaystyle\int_L \mathbf{C}_\alpha^\mathrm{T} D\,H_n\,\mathrm{d}L \\ \hline \displaystyle\int_L \left(H_\beta + S_\mathrm{v} S_\mathrm{N}\mu|\kappa|\tilde{L}_\beta\right) D\,\mathbf{C}_k\,\mathrm{d}L & \displaystyle\int_L \left(H_\beta + S_\mathrm{v} S_\mathrm{N}\mu|\kappa|\tilde{L}_\beta\right) D\,H_n\,\mathrm{d}L \end{array}\right] \left[\begin{array}{c} \Delta\mathbf{q}_k \\ \hline \Delta v_n \end{array}\right]$$

$$= \left[\begin{array}{c} \displaystyle\int_V \mathbf{L}_\alpha^\mathrm{T}\,(\mathbf{Q}+\Delta\mathbf{Q})\,\mathrm{d}V - \int_V \mathbf{B}_\alpha^\mathrm{T}\boldsymbol{\sigma}\,\mathrm{d}V - \int_L \mathbf{C}_\alpha^\mathrm{T} N\,\mathrm{d}L \\ \hline \displaystyle\int_L \tilde{L}_\beta\,(P+\Delta P)\,\mathrm{d}L - \int_L \left(H_\beta + \tilde{L}_\beta\mu|\kappa| S_v S_\mathrm{N}\right) N\,\mathrm{d}L - \int_L \tilde{L}_\beta S_v T_0\,\mathrm{d}L \end{array}\right] \tag{39}$$

which is used to assemble the global finite element equation system. The system is not symmetrical and nonlinear. The Newton–Raphson incremental-iterative procedure is employed to obtain solution. Because Eq. (39) is incremental, we may treat the right hand side of it as a residual vector that we want to be zero. In Eq. (39), components integrated over volume V come from the parent element whereas the emebedded element contributes in integrals over length L. The slip degrees are treated as global to ensure compatibility of displacement between adjacent tendon elements. Since friction is taken into consideration at these degrees, we must first determine whether the slip is possible or not. The following procedure is proposed.

Let I mean the global I^{th} tendon node and associated slip degree of freedom. The corresponding element of the residual vector that is zero at equilibrium may be written as

$$\sum_{(e)} \Omega_I^{\beta(e)} \left(\int_L \left[\tilde{L}_\beta (P + \Delta P) - H_\beta N \right] \mathrm{d}L - \psi \int_L \left[\tilde{L}_\beta \mu |\kappa| + \tilde{L}_\beta S_\mathrm{N} T_0 \right] \mathrm{d}L \right)^{(e)} = 0 , \tag{40}$$

where $\Omega_I^{\beta(e)}$ denotes the incidence matrix, (e) means summation over tendon elements adjacent to I, and $\psi = S_v S_\mathrm{N}$ with obvious identity $S_\mathrm{N} = 1/S_\mathrm{N}$. Factor S_N should be equal to $+1$ since we want to have tension in prestressing tendons but it is not skipped for the sake of clarity. In the numerical solution S_v is identified with the sign of Δv. Both S_v and S_N are determined at the beginning of each increment in one additional iteration where friction is neglected just to estimate the tendency of the system. This iteration is referred to as director. Then at each slip degree of freedom Eq. (40) is solved for ψ. Thus

$$\psi = \frac{\displaystyle\sum_{(e)} \Omega_I^{\beta(e)} \left(\int_L \left[\tilde{L}_\beta (P + \Delta P) - H_\beta N \right] \mathrm{d}L \right)^{(e)}}{\displaystyle\sum_{(e)} \Omega_I^{\beta(e)} \left(\int_L \left[\tilde{L}_\beta \mu |\kappa| + \tilde{L}_\beta S_\mathrm{N} T_0 \right] \mathrm{d}L \right)^{(e)}} , \tag{41}$$

where we have the nodal equivalent of friction force in the denominator and the nodal equivalent of external and internal forces in the numerator. Equation (25) is derived for kinematically admissible variations of $\delta \Delta v$ meaning that friction force reaches the limit value T, which corresponds to $|\psi| = 1$. Hence, if we get $|\psi| < 1$ then the friction force is less then the limit value and no slip can occur so additional boundary condition is introduced. On the other hand, if $|\psi| > 1$ then ψ is set to $S_v S_\mathrm{N}$ and the possibility of movement remains or is restored if it was restrained earlier. The slip is also possible if $|\psi| = 1$ and $\psi = S_v S_\mathrm{N}$. But if $|\psi| = 1$ and $\psi = -S_v S_\mathrm{N}$ no slip can occur. With boundary conditions modified that way the next iteration called predictor is performed after which ψ is recalculated from (41) to check if any change in additional boundary conditions is encountered. The predictor is repeated until no change occurs. Then, next iterations called correctors are performed to make the residua zero.

3. Implementation

The tendon element derived in previous section can be embedded potentially in any type of parent element. So far it has been successfully applied with standard beam, shell and volume elements. Derivation of parent elements is skipped because it leads to the formulation of well-known standard elements that can be found for example in [19]. Only quantities needed for the geometrical description of the embedded element are briefly outlined. To help comprehend the main concept of the model, more details are given for prestressed beam being the simplest application of the developed model.

3.1. Beams

A standard, straight, two noded beam element with three degrees of freedom at a node $\mathbf{q}_i = \{u_i\,,\, w_i\,,\, \varphi_i\}^{\mathrm{T}}$ is considered as a parent element in which a tendon element is embedded (Fig. 1).

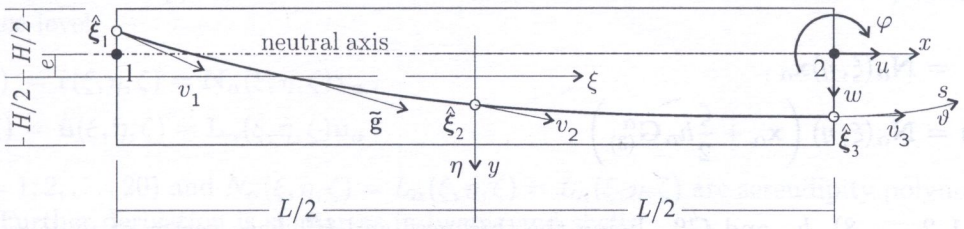

Fig. 1. Prestressed beam model

For convenience, the local coordinate system $\{\xi, \eta\}$ of the parent element is positioned at the center of the beam element wheras the global reference system $\{x, y\}$ is aligned with the neutral axis. Thus, the position radius-vectors equal

$$\mathbf{r}(\xi) = N_1(\xi)\mathbf{x}_1 + N_2(\xi)\mathbf{x}_2 = \frac{1-\xi}{2}\{-L/2\,,\, 0\}^{\mathrm{T}} + \frac{1+\xi}{2}\{L/2\,,\, 0\}^{\mathrm{T}} = \left\{\frac{L}{2}\xi, 0\right\}^{\mathrm{T}}, \tag{42}$$

$$\hat{\mathbf{r}}(\xi,\eta) = \{x(\xi), y(\eta)\}^{\mathrm{T}} = \left\{\frac{L}{2}\xi\,,\, \frac{H}{2}\eta + e\right\}^{\mathrm{T}}, \tag{43}$$

with ξ and η running from -1 to $+1$ and e being the eccentricity between the middle and the neutral axes. Deformation of the neutral axis is described by vector

$$\begin{aligned}\mathbf{u}(\xi) &= \{u(\xi), w(\xi)\}^{\mathrm{T}} = \mathbf{L}_1(\xi)\mathbf{q}_1 + \mathbf{L}_2(\xi)\mathbf{q}_2 \\ &= \begin{bmatrix} h_1(\xi) & 0 & 0 \\ 0 & h_2(\xi) & h_3(\xi) \end{bmatrix}\mathbf{q}_1 + \begin{bmatrix} h_4(\xi) & 0 & 0 \\ 0 & h_5(\xi) & h_6(\xi) \end{bmatrix}\mathbf{q}_2\,,\end{aligned} \tag{44}$$

which is interpolated between nodes with hermitian shape functions $h_i(\xi)$. To obtain displacement of any point $\hat{\mathbf{u}}(\xi,\eta)$, the rotation of section $\varphi = \frac{\mathrm{d}w}{\mathrm{d}x}$ must be taken into account. Thus

$$\begin{aligned}\hat{\mathbf{u}}(\xi,\eta) &= \{u(\xi) - \varphi(\xi)y(\eta), w(\xi)\}^{\mathrm{T}} = \hat{\mathbf{L}}_1(\xi,\eta)\mathbf{q}_1 + \hat{\mathbf{L}}_2(\xi,\eta)\mathbf{q}_2 \\ &= \begin{bmatrix} h_1(\xi) & -h_{2,x}y(\eta) & -h_{3,x}y(\eta) \\ 0 & h_2(\xi) & h_3(\xi) \end{bmatrix}\mathbf{q}_1 + \begin{bmatrix} h_4(\xi) & -h_{5,x}y(\eta) & -h_{6,x}y(\eta) \\ 0 & h_5(\xi) & h_6(\xi) \end{bmatrix}\mathbf{q}_2\,,\end{aligned} \tag{45}$$

where $h_{i,x}$ are derivatives of h_i with respect to x. Now if we assume that nodal coordinates $\hat{\boldsymbol{\xi}}_i = \{\hat{\xi}_i\,,\, \hat{\eta}_i\}^{\mathrm{T}}$ of the emebedded tendon element are known, then the tendon line is approximated according to Eq. (8)

$$\tilde{\boldsymbol{\xi}}(\vartheta) = \{\tilde{\xi}(\vartheta)\,,\, \tilde{\eta}(\vartheta)\}^{\mathrm{T}} = \tilde{N}_1(\vartheta)\{\hat{\xi}_1\,,\, \hat{\eta}_1\}^{\mathrm{T}} + \tilde{N}_2(\vartheta)\{\hat{\xi}_2\,,\, \hat{\eta}_2\}^{\mathrm{T}} + \tilde{N}_3(\vartheta)\{\hat{\xi}_3\,,\, \hat{\eta}_3\}^{\mathrm{T}}, \tag{46}$$

in local coordinates of the parent element. This approximation is used to obtain global coordinates $\tilde{\mathbf{r}}(\vartheta)$ from Eq. (43)

$$\tilde{\mathbf{r}}(\vartheta) = \hat{\mathbf{r}}(\tilde{\xi}(\vartheta)\,,\, \tilde{\eta}(\vartheta)) = \{\tilde{x}(\xi(\vartheta))\,,\, \tilde{y}(\eta(\vartheta))\}^{\mathrm{T}} = \left\{\frac{L}{2}\tilde{\xi}(\vartheta)\,,\, \frac{H}{2}\tilde{\eta}(\vartheta) + e\right\}^{\mathrm{T}}, \tag{47}$$

so $\frac{\mathrm{d}s}{\mathrm{d}\vartheta}$, $\tilde{\mathbf{g}}$ and $\tilde{\mathbf{n}}$ can be calculated which are needed to have the curvature $|\tilde{\kappa}|$ and matrices $\mathbf{C}$ and $\mathbf{H}$ defined by Eqs. (13), (17) and (18) respectively. Hence we obtain all quantities to build the FEM equation system.

3.2. Shells

For modeling prestressed shells (Fig. 2), the widely used isoparametric curved elements with five degrees of freedom at a node are employed [1, 14, 20]. The approximation of shell element geometry is given by

$$\mathbf{r}(\xi,\eta) = \mathbf{N}_\alpha(\xi,\eta)\mathbf{x}_\alpha\,, \tag{48}$$

$$\hat{\mathbf{r}}(\xi,\eta,\zeta) = \mathbf{N}_\alpha(\xi,\eta)\left(\mathbf{x}_\alpha + \frac{\zeta}{2}h_\alpha \mathbf{G}^\alpha_{\langle 3\rangle}\right), \tag{49}$$

with $(\alpha = 1,2,\ldots,8)$, h_α and $\mathbf{G}^\alpha_{\langle k\rangle}$ being the thickness and k^{th} base vector at node α. The same serendipity polynomial shape functions $N_\alpha(\xi,\eta) = L_\alpha(\xi,\eta)$ are used to approximate the displacement field of any shell point

$$\hat{\mathbf{u}}(\xi,\eta,\zeta) = \sum_\alpha \mathbf{N}_{(\alpha)}(\xi,\eta)\left(\mathbf{u}_{(\alpha)} + \frac{\zeta}{2}h_{(\alpha)}[-\mathbf{G}^{(\alpha)}_{\langle 2\rangle}\,,\ \mathbf{G}^{(\alpha)}_{\langle 1\rangle}]\{\omega_{\langle 1\rangle}\,,\ \omega_{\langle 2\rangle}\}^{\mathrm{T}}_{(\alpha)}\right) = \hat{\mathbf{L}}_\alpha \mathbf{q}_\alpha\,, \tag{50}$$

where $\mathbf{q}_i = \{u_1\,,\ u_2\,,\ u_3\,,\ \omega_{\langle 1\rangle}\,,\ \omega_{\langle 2\rangle}\}^{\mathrm{T}}_\alpha$ is a set of nodal parameters conforming to five-parameter shell theory with translations u_i defined in the global system and $\omega_{\langle j\rangle}$ being physical coordinates of the angle rotation vector. Matrix $\hat{\mathbf{L}}_\alpha$ is equal to

$$\hat{\mathbf{L}}_\alpha(\xi,\eta,\zeta) = N_{(\alpha)}(\xi,\eta)\begin{bmatrix} 1 & 0 & 0 & -\frac{\zeta}{2}h_{(\alpha)}G^{(\alpha)}_{\langle 2\rangle 1} & \frac{\zeta}{2}h_{(\alpha)}G^{(\alpha)}_{\langle 1\rangle 1} \\ 0 & 1 & 0 & -\frac{\zeta}{2}h_{(\alpha)}G^{(\alpha)}_{\langle 2\rangle 2} & \frac{\zeta}{2}h_{(\alpha)}G^{(\alpha)}_{\langle 1\rangle 2} \\ 0 & 0 & 1 & -\frac{\zeta}{2}h_{(\alpha)}G^{(\alpha)}_{\langle 2\rangle 3} & \frac{\zeta}{2}h_{(\alpha)}G^{(\alpha)}_{\langle 1\rangle 3} \end{bmatrix}. \tag{51}$$

Introducing the approximation of the tendon line

$$\tilde{\boldsymbol{\xi}}(\vartheta) = \{\tilde{\xi}(\vartheta)\,,\ \hat{\eta}(\vartheta)\,,\ \hat{\zeta}(\vartheta)\}^{\mathrm{T}} = \tilde{N}_1(\vartheta)\{\hat{\xi}_1\,,\ \hat{\eta}_1\,,\ \hat{\zeta}_1\}^{\mathrm{T}} + \tilde{N}_2(\vartheta)\{\hat{\xi}_2\,,\ \hat{\eta}_2\,,\ \hat{\zeta}_2\}^{\mathrm{T}} + \tilde{N}_3(\vartheta)\{\hat{\xi}_3\,,\ \hat{\eta}_3\,,\ \hat{\zeta}_3\}^{\mathrm{T}}, \tag{52}$$

to $\hat{\mathbf{r}}$ and $\hat{\mathbf{L}}$ defined by Eqs. (49) and (51) enables formulation of a tendon element embedded in a shell element.

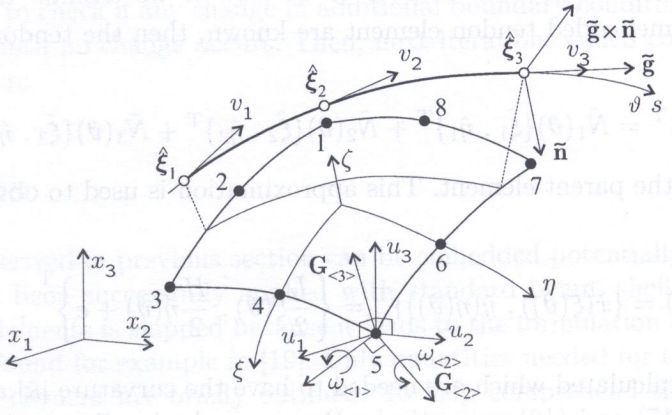

Fig. 2. Prestressed shell model

3.3. Volumes

Three-dimensional prestressed structures are modeled with 20-node curved isoparametric elements with three translational degrees of freedom at a node (Fig. 3). For this type of element geometry and displacements are approximated in the same way with no distinction between points on and off the reference level

$$\mathbf{r}(\xi,\eta,\zeta) = \hat{\mathbf{r}}(\xi,\eta,\zeta) = \mathbf{N}_\alpha(\xi,\eta,\zeta)\mathbf{x}_\alpha\,, \tag{53}$$

$$\mathbf{u}(\xi,\eta,\zeta) = \hat{\mathbf{u}}(\xi,\eta,\zeta) = \mathbf{L}_\alpha(\xi,\eta,\zeta)\mathbf{u}_\alpha\,, \tag{54}$$

where $(\alpha = 1,2,\ldots,20)$ and $N_\alpha(\xi,\eta,\zeta) = L_\alpha(\xi,\eta,\zeta) = \hat{L}_\alpha(\xi,\eta,\zeta)$ are serendipity polynomial shape functions. Further derivation is similar as in beams and shells.

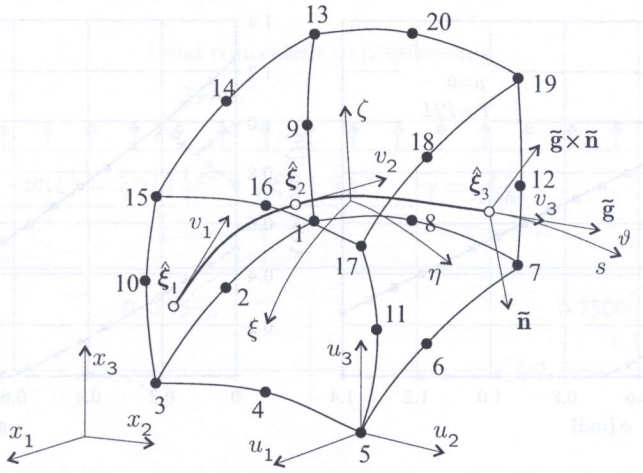

Fig. 3. Prestressed volume model

4. Numerical examples

4.1. Tendon with friction

The capability of modeling friction is tested on a single circular tendon in a stiff duct. For this purpose a model consisting of one parent shell element with ten embedded tendon elements is analyzed (Fig. 4). All parent element degrees of freedom are restrained to model the stiff duct. The tendon slip is restrained at one end and loading is applied at the other one. Four subsequent load increments are applied to model tensioning $(+0.50P, +0.75P)$, untensioning $(-0.50P)$ and re-tensioning $(+0.25P)$ giving the final prestressing force P.

This simple example can be solved analytically. Knowing that $T = \frac{\mathrm{d}N}{\mathrm{d}s}$ we may solve Eq. (24) for N which for a prestressing force S gives

$$N(s) = Se^{-\mu\kappa s} - \frac{T_0}{\kappa\mu}\left(1 - e^{-\mu\kappa s}\right)\,, \tag{55}$$

or in terms of $\phi = s\kappa$ (with $\hat{\kappa} = 0$)

$$N(\phi) = Se^{-\mu\phi} - \frac{T_0}{\kappa\mu}\left(1 - e^{-\mu\phi}\right)\,. \tag{56}$$

In particular for $T_0 = 0$ we get the well known formula

$$N(\phi) = Se^{-\mu\phi}\,, \tag{57}$$

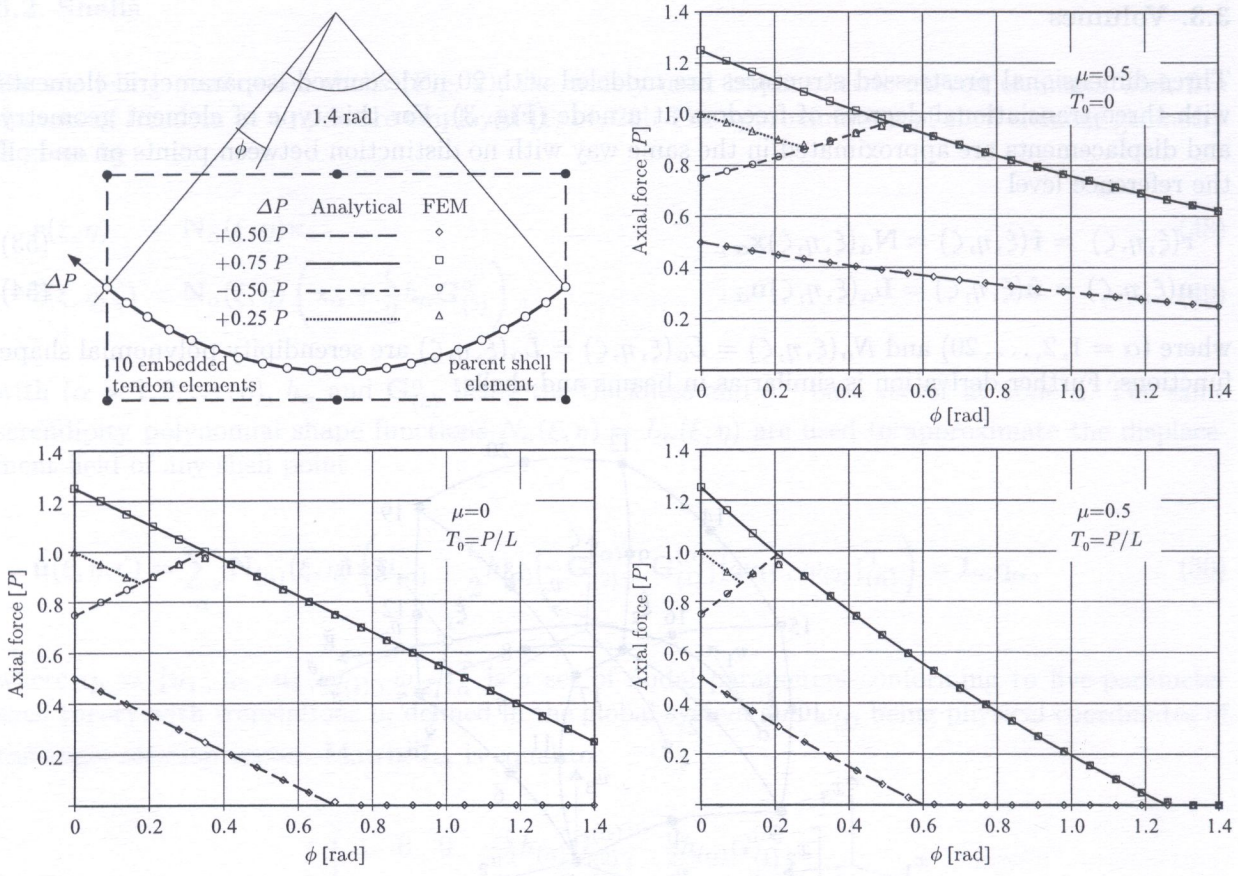

Fig. 4. Numerical example 1: Mesh and tendon axial forces

and for $\mu = 0$

$$N(\phi) = \lim_{\mu \to 0} \left(S e^{-\mu\phi} - \frac{T_0}{\kappa\mu} \left(1 - e^{-\mu\phi} \right) \right) = S - \frac{T_0 \phi}{\kappa} \,. \tag{58}$$

Due to the nature of friction these solutions may apply only to a limited zone of the tendon. Caution must be taken especially in case of untensioning and re-tensioning where further derivation is necessary.

Three cases were considered in this example, all with $\hat{\kappa} = 0$, namely

$$\begin{aligned} &(\mu = 0.5,\ T_0 = 0) && \Rightarrow \quad N(\phi) = S e^{-0.5\phi} \,, \\ &(\mu = 0, \quad T_0 = P/L) && \Rightarrow \quad N(\phi) = S(1 - \phi/1.4) \,, \\ &(\mu = 0.5,\ T_0 = P/L) && \Rightarrow \quad N(\phi) = S e^{-0.5\phi} - \frac{P}{0.7} \left(1 - e^{-0.5\phi} \right) , \end{aligned} \tag{59}$$

where $N(\phi)$ is the axial force distribution for tensioning stage ($S = 0.25P$, $S = 1.25P$).

Complete analytical solutions are presented by lines on the charts in Fig. 4 whereas the finite element results are shown by markers representing nodal values of axial forces. Very good agreement between the analytical and numerical solutions is observed.

4.2. Statically indetermined prestressed beam

A prestressed beam (Fig. 5a) analyzed also in [4] is used to test the finite element beam and volume models. Friction is neglected in this example. The results shown in (Fig. 5c) and (Fig. 5d) are in good agreement with the analytical solution obtained with the load equivalent method (Fig. 5b).

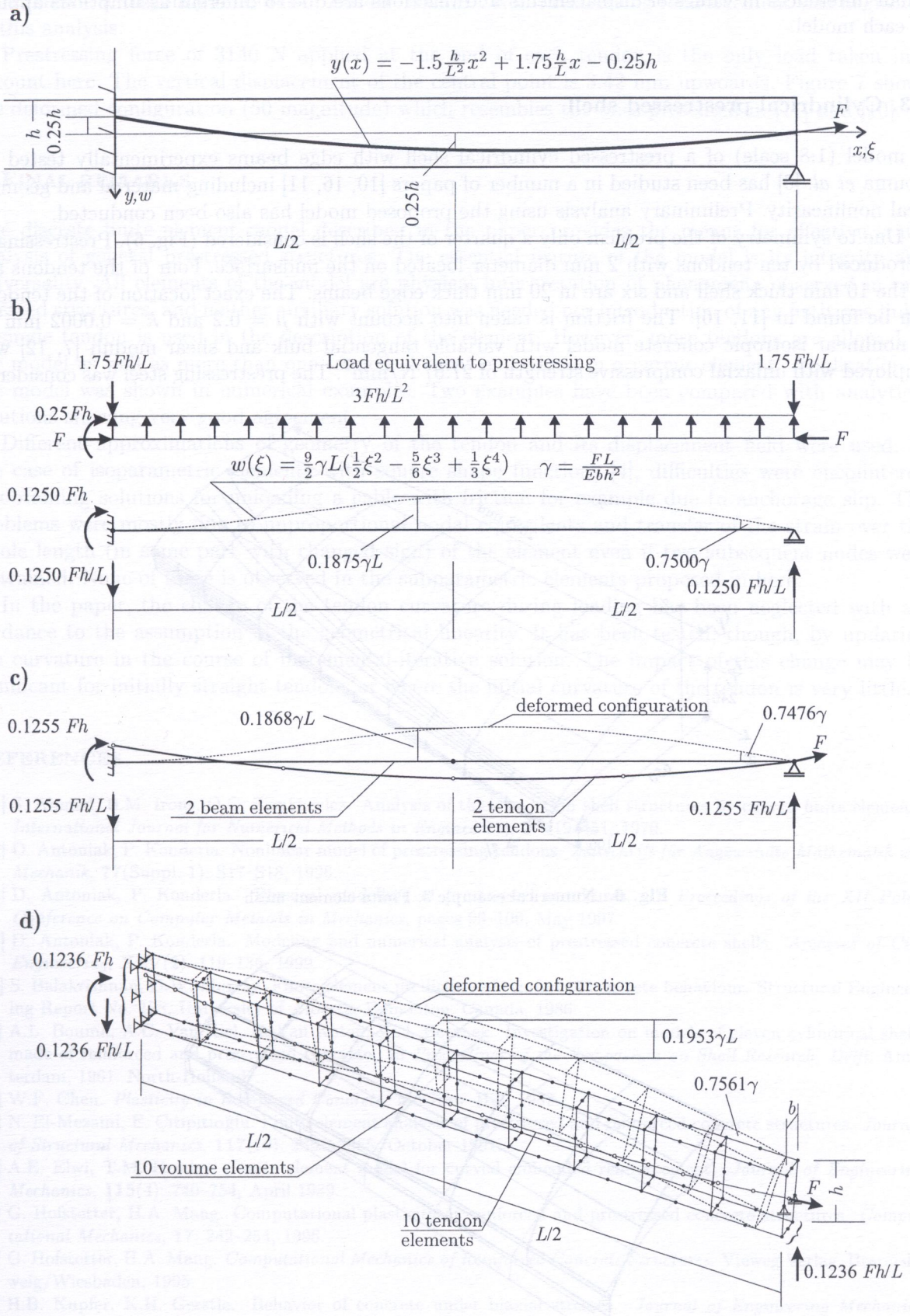

Fig. 5. Numerical example 2: a) Problem formulation, b) analytical beam solution, c) FEM beam solution, d) FEM volume solution

Small differences in values of displacements and reactions are due to different assumptions applied in each model.

4.3. Cylindrical prestressed shell

A model (1:8 scale) of a prestressed cylindrical shell with edge beams experimentally tested by Bouma *et al.* [6] has been studied in a number of papers [10, 16, 11] including material and geometrical nonlinearity. Preliminary analysis using the proposed model has also been conducted.

Due to symmetry of the problem only a quarter of the shell is considered (Fig. 6). Prestressing is introduced by ten tendons with 2 mm diameter located on the midsurface. Four of the tendons are in the 10 mm thick shell and six are in 20 mm thick edge beams. The exact location of the tendons can be found in [11, 16]. The friction is taken into account with $\mu = 0.2$ and $\hat{\kappa} = 0.0002$ mm^{-1}. A nonlinear isotropic concrete model with variable tangential bulk and shear moduli [7, 12] was employed with uniaxial compressive strength of 27.67 N/mm^2. The prestressing steel was considered

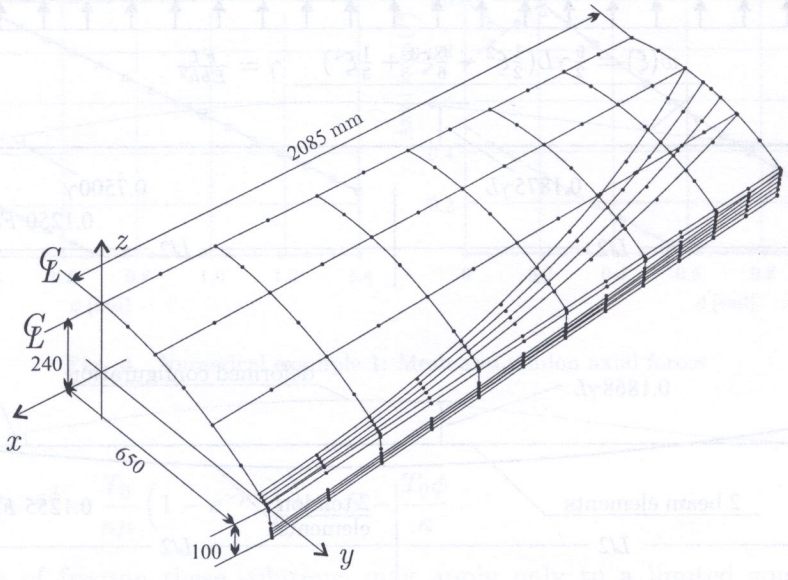

Fig. 6. Numerical example 3: Finite element mesh

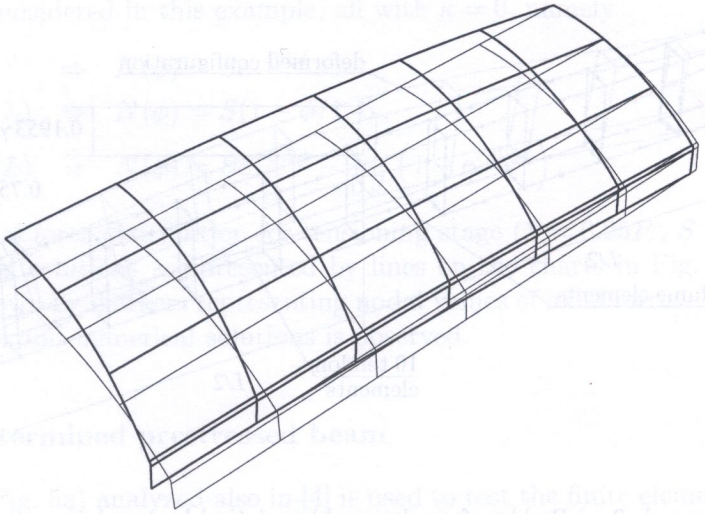

Fig. 7. Numerical example 3: Deformation due to prestressing

linear elastic with young modulus of $2.0 \cdot 10^5$ N/mm^2. Non-prestressing reinforcement was neglected in this analysis.

Prestressing force of 3140 N applied at the end of each tendon is the only load taken into account here. The vertical displacement of the central point is 3.42 mm upwoards. Figure 7 shows the deformed configuration (50 magnitude) which resembles the ones presented in [11] and [10].

5. Final remarks

The discrete finite element model described in the paper provides the means for effective static analysis of general prestressed structures. The essential feature of the model is its integrity and universality. All elements of the model are physical interpretation of phenomena observed in prestressed structures, and neither auxiliary solution was needed nor introduction of any fictitious links. A single tendon is used in the description of the element. However, more tendons are allowed in the model as well as more than one tendon element embedded in a parent element. Application of the model was shown in numerical examples. Two examples have been compared with analytical solutions showing very good agreement.

Different approximations of geometry of the tendon and its displacement field were used. In the case of isoparametric elements with square shape functions [4], difficulties were encountered in obtaining solutions for unloading a cable with friction for example due to anchorage slip. The problems were mostly due to unproportional nodal equivalents and transfer of the strain over the whole length (in some part with changed sign) of the element even if two subsequent nodes were restrained. None of these is observed in the subparametric elements proposed in here.

In the paper, the change of the tendon curvature during loading has been neglected with accordance to the assumption of the geometrical linearity. It has been tested, though, by updating the curvature in the course of incremental-iterative solution. The impact of this change may be significant for initially straight tendons or where the initial curvature of the tendon is very little.

References

[1] S. Ahmad, B.M. Irons, O.C. Zienkiewicz. Analysis of thick and thin shell structures by curved finite elements. *International Journal for Numerical Methods in Engineering*, **2**: 419–451, 1970.

[2] D. Antoniak, P. Konderla. Nonlinear model of prestressing tendons. *Zeitschrift für Angewandte Mathematik und Mechanik*, **77**(Suppl. 1): S17–S18, 1996.

[3] D. Antoniak, P. Konderla. Physical modelling of prestressed structures. In *Proceedings of the XII Polish Conference on Computer Methods in Mechanics*, pages 99–106, May 1997.

[4] D. Antoniak, P. Konderla. Modeling and numerical analysis of prestressed concrete shells. *Archives of Civil Engineering*, **XLV**(2): 119–136, 1999.

[5] S. Balakrishnan, D.W. Murray. Finite element prediction of reinforced concrete behaviour. Structural Engineering Report No. 138, University of Alberta, Edmonton, Canada, 1986.

[6] A.L. Bouma, A.C. Van Riel, H. Van Koten, W.J. Beranek. Investigation on models of eleven cylindrical shells made of reinforced and prestressed concrete. In *Proceedings of the Symposium on Shell Research, Delft*, Amsterdam, 1961. North-Holland.

[7] W.F. Chen. *Plasticity in Reinforced Concrete.* McGraw–Hill, 1982.

[8] N. El-Mezaini, E. Çıtıpıtıoğlu. Finite element analysis of prestressed and reinforced concrete structures. *Journal of Structural Mechanics*, **117**(10): 2851–2865, October 1991.

[9] A.E. Elwi, T.M. Hrudey. Finite element model for curved embedded reinforcement. *Journal of Engineering Mechanics*, **115**(4): 740–754, April 1989.

[10] G. Hofstetter, H.A. Mang. Computational plasticity of reinforced and prestressed concrete structures. *Computational Mechanics*, **17**: 242–254, 1996.

[11] G. Hofstetter, H.A. Mang. *Computational Mechanics of Reinforced Concrete Structures.* Vieweg Verlag, Braunshweig/Wiesbaden, 1995.

[12] H.B. Kupfer, K.H. Gerstle. Behavior of concrete under biaxial stresses. *Journal of Engineering Mechanics Division*, **99**(EM4): 852–866, August 1973.

[13] H.A. Mang, G. Menschke. Nonlinear finite element analysis of reinforced and prestressed concrete structures. *Engineering Structures*, **13**(2): 211–226, April 1991.

[14] S.F. Pawsey, R.W. Clough. Improved numerical integration of thick shell finite elements. *International Journal for Numerical Methods in Engineering*, **3**: 575–586, 1971.

[15] D.V. Philips, O.C. Zienkiewicz. Finite element non-linear analysis of concrete structures. *Proceedings of Institute of Civil Engineering*, **61**(1): 59–88, 1976.

[16] P. Roca, A.R. Marí. Nonlinear geometric and material analysis of prestressed concrete general shell structures. *Computers and Structures*, **46**(5): 917–929, 1993.

[17] P. Roca, A.R. Marí. Numerical treatment of prestressing tendons in the nonlinear analysis of prestressed concrete structures. *Computers and Structures*, **46**(5): 905–916, 1993.

[18] A.C. Scordelis. Computer models for nonlinear analysis of reinforced and prestressed concrete structures. *PCI Journal*, 116–135, November-December 1984.

[19] O.C. Zienkiewicz, R.L. Taylor. *Finite element method.* McGraw–Hill Book Company, London, 4'th edition, 1989.

[20] O.C. Zienkiewicz, R.L. Taylor, J.M. Too. Reduced integration technique in general analysis of plates and shells. *International Journal for Numerical Methods in Engineering*, **3**: 275–290, 1971.